Chemical Science

ROYAL SOCIETY OF CHEMISTRY

EDGE ARTICLE

View Article Online
View Journal | View Issue

Cite this: *Chem. Sci.*, 2026, **17**, 2712

All publication charges for this article have been paid for by the Royal Society of Chemistry

Regulation and mechanisms of full-visible-spectrum emission in solid and liquid states for D-π-A cyanobenzene–phenothiazine fluorescent molecules

Wen-Hao Li,[a] Meng-Yao Niu,[a] Yi-Yun Zhu,[a] Man Zhang,[a] Hao-Yu Gao,[d] Xin-Chao Zhang,[a] Bo Yang, *[a] Donghui Wei *[a] and Xuenian Chen *[abc]

The precise modulation of photophysical properties and elucidation of fluorescence mechanisms are paramount challenges for organic optoelectronic materials. Herein, we present a strategy for achieving robust fluorescence tuning from blue (462 nm) to near-infrared (677 nm) by accurately positioning electron-withdrawing groups relative to phenothiazine donors in cyanobenzene–phenothiazine derivatives, as well as adjusting molecular conformations, noncovalent interactions, and the interplays of aggregation behaviors. Crystallographic analysis and theoretical calculations revealed that 4-phenothiazino-isophthaliconitrile (**4-PTZIPN**) achieves both the highest solid-state fluorescence quantum yield (39.7%) and the longest fluorescence lifetime (1.26 μs) among the series, which is attributed to J-aggregation sustained by multiple intermolecular interactions. The conformation and rigidified non-canonical J-aggregation suppressed non-radiative decay pathways, leading to a significant increase in the quantum yield of 2,4,6-triphenothiazinobenzonitrile (**1CN3PTZ**) and a substantial extension of its fluorescence lifetime from 761.47 ns in the solid-state to 1.10 μs. Notably, 2,4,6-triphenothiazino-isophthaliconitrile (**2CN3PTZ**) demonstrates a pronounced bathochromic shift to 677 nm, driven by its helical columnar packing, which is orchestrated by cooperative π–π, dipole–dipole, and C–H···S interactions. This work not only elucidated the structure–photophysical relationships within the cyano-phenothiazine system but also provided a conformation-aggregation dual regulation strategy for the design of innovative organic optoelectronic materials through molecular engineering.

Received 11th August 2025
Accepted 29th November 2025

DOI: 10.1039/d5sc06095h

rsc.li/chemical-science

Introduction

The development of organic luminescent materials capable of spanning the entire visible spectrum (400–700 nm) is critical for advanced optoelectronic applications, from full-color displays to biological imaging.[1–3] Donor–acceptor (D–A) systems offer a powerful platform for tunable emission through intramolecular charge transfer (ICT).[4–10] Despite these advantages, the existing D–A materials face two challenges: (1) limited solid-state emission range due to aggregation-caused quenching (ACQ), and (2) unresolved correlations between molecular conformation, packing motifs, and photophysical outcomes. Addressing these limitations requires innovative molecular engineering that synergistically considers electronic structures and aggregation behaviors—an unmet goal that underpins the significance of this work.

The flexible butterfly-like conformations of phenothiazine enable dynamic control of molecular planarity and packing, and its electron-rich nature confers exceptional charge transport capabilities, resulting in diverse applications across chemical sensing,[11] organic optoelectronics,[12] bioimaging,[13–16] organic photovoltaics,[17–21] and organocatalysis.[22–37] The cyano group, serving as an electron acceptor, not only participates in the conjugated system through its π* antibonding orbitals to lower the lowest unoccupied molecular orbital (LUMO) energy level,[3,38–42] thereby enhancing intramolecular charge transfer (ICT) but also enables precise molecular assembly *via* directional dipole–dipole interactions (*e.g.*, C≡N···H–C, C≡N···π).[43–46] To our knowledge, only a few literature reports describe the molecular fluorescence of 4-CN-PTH,[47–52] and no studies have extended to investigate structures with increased numbers of donor–acceptor pairs and their properties. In this work,

[a]*College of Chemistry, Zhengzhou University, Zhengzhou, Henan 450001, China. E-mail: yangbohy@zzu.edu.cn; donghuiwei@zzu.edu.cn; xuenian_chen@zzu.edu.cn*

[b]*School of Chemistry and Chemical Engineering, Henan Key Laboratory of Boron Chemistry and Advanced Materials, Henan Normal University, Xinxiang, Henan 453007, China*

[c]*State Key Laboratory of Coordination Chemistry, School of Chemistry and Chemical Engineering, Nanjing University, Nanjing 210093, China*

[d]*College of Science, Henan Agricultural University, Zhengzhou, Henan 450002, China*

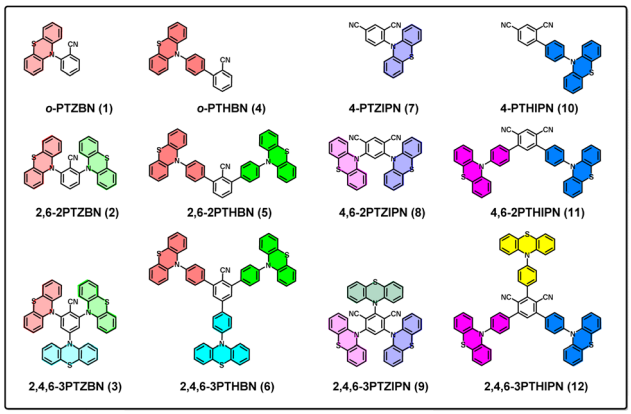

Fig. 1 Numbers and structures of cyanobenzene phenothiazine derivatives **1–12**.

based on the ***o*-PTZBN** (**1**) molecular framework, we maintained the adjacent relative positioning of cyano and phenothiazine groups on the central benzene ring to design and synthesize a series of cyanobenzene phenothiazine derivatives by systematically increasing the total number of adjacent donor–acceptor pairs. Combining X-ray diffraction and photophysical characterization, we implemented a "dual-control strategy for conformation and packing" to achieve full-spectrum visible-light emission in both solution and solid states. Furthermore, we systematically investigated the structure–property relationship between molecular packing modes and fluorescence performance of such D–A systems in rigid crystalline states, providing new insights for structure-guided luminescence regulation (Fig. 1).

Results and discussion

As shown in Scheme 1, **PTZBNs** (**1–3**) and **PTZIPNs** (**7–9**) were successfully synthesized through two complementary synthetic routes, aromatic nucleophilic substitution (S_NAr) and Buchwald–Hartwig amination. Among them, the 2,4,6-triphenothiazinylisophthalonitrile (**9**) was efficiently accessed using *rac*-BI-DIME as the phosphine ligand,[53] the palladium acetate as the catalyst, and the 2,4,6-3BrIPN as the starting material. In addition, **PTH-Bpin** was synthesized *via* Sandmeyer borylation, and **PTHBNs** (**4–6**) and **PTHIPNs** (**10–12**) were

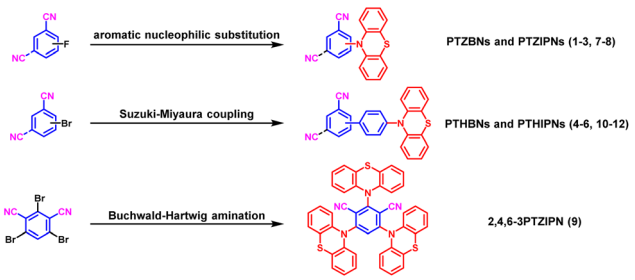

Scheme 1 Synthetic routes of cyanobenzene phenothiazine derivatives **1–12**.

synthesized *via* Suzuki–Miyaura coupling. Their structure-dependent photophysical properties, spanning solution-phase tunability (503–651 nm) to solid-state full-spectrum emission (462–677 nm), along with intermolecular interaction-directed packing modes, are systematically presented below. Unfortunately, attempts to synthesize 4PTZIPN from 2,4,5,6-4FIPN were unsuccessful, potentially due to the steric hindrance and the poor solubility of the 5-F-3PTZIPN intermediate.[54] The thermodynamic instability of the 1,3,5-tricyanobenzene core under palladium-catalyzed conditions may hinder the synthesis of 3CN3PTZ and 3CN3PTH *via* 3Br3CN coupling. The detailed characterization information of all **1–12** compounds is provided in the SI (Fig. S1–S94).

Solubility profiling showed complete dissolution of all derivatives **1–12** in nonpolar solvents (dichloromethane, chloroform, toluene) and polar aprotic solvents (acetonitrile, DMSO, DMF), but insolubility in protic solvents (acetic acid, methanol, ethanol). UV-vis absorption spectra of **1-12** in toluene revealed distinct absorption peaks at 305 nm (**1**), 308 nm (**2**), 315 nm (**3**), 320 nm (**4**), 305 nm (**5**), 298 nm (**6**), 294 nm (**7**), 296 nm (**8**), 284 nm (**9**), 357 nm (**10**), 371 nm (**11**), and 371 nm (**12**), suggesting that substituent groups, positions, and quantities profoundly alter optical properties (Fig. S107). To further study their optical properties in solution and in ICT, we measured the fluorescence spectra in various solvents with the same concentration (Fig. S123 and S124) and in toluene with different concentrations (Fig. S125 and S126). Notably, these compounds exhibit significant fluorescence emission only in toluene (under 365 nm UV light). Specifically, in dilute toluene solutions (1×10^{-6} M), only short-wavelength emission peaks (410–420 nm) are observed; however, as the concentration increases ($>1 \times 10^{-4}$ M), long-wavelength emission peaks become dominant. Thus, we conclude that the full-spectrum emission of these compounds in toluene originates from their aggregation behavior. Their maximum fluorescence emission in toluene solution showed bathochromic shifts across a broad range from 503 to 651 nm (Fig. 2a and b), which further confirms the tunability of their structure–activity relationship. Among them, **9** with the highest density of interdigitated donor–acceptor alternations exhibit the most significant emission red-shift.

The Lippert–Mataga plot (Fig. 3) reveals that the solvent-dependent Stokes shift of all derivatives correlates with the solvent orientation polarizability (Δf), where the slope directly reflects the magnitude of the dipole moment difference ($\Delta\mu$) between the excited state and the ground state. Specifically, **PTZBNs** (**1–3**), **PTZIPNs** (**7–9**), and **PTHBNs** (**4–6**) exhibit comparable slopes, respectively, indicating that derivatives within each series possess similar $\Delta\mu$ due to consistent charge transfer pathways mediated by their conjugated frameworks. In contrast, the **PTHIPNs** (**10–12**) series exhibits distinct slope variations, with compound **12**, which has a larger molecular size due to the introduction of three PTH moieties on its central dicyanobenzene ring, displaying the lowest slope. This divergence arises because the addition of these three PTH moieties fails to enhance $\Delta\mu$ effectively, as the phenylene bridging group in PTHIPNs may not participate in excited-state electron transfer, thereby restricting the extension of charge

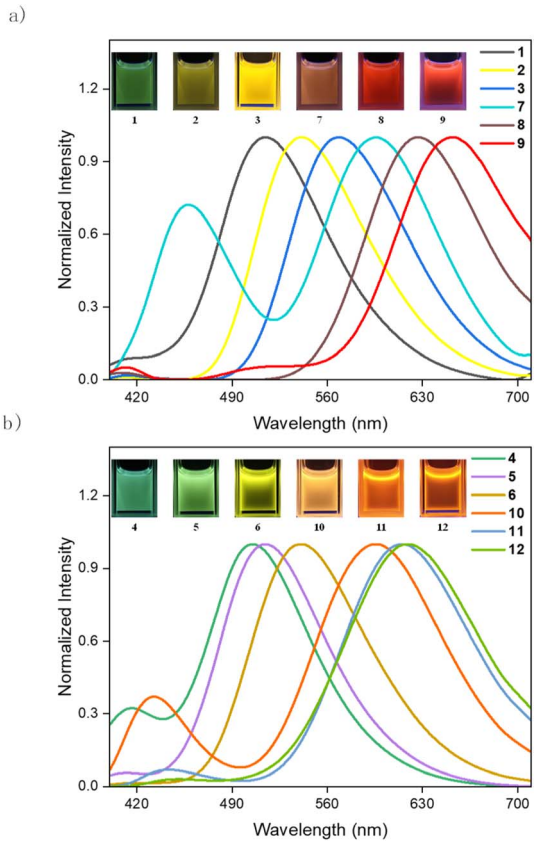

Fig. 2 (a) Solution-state fluorescence emission spectrum of **PTZBNs** (**1–3**) and **PTZIPNs** (**7–9**) in toluene; (b) solution-state fluorescence emission spectrum of **PTHBNs** (**4–6**) and **PTZIPNs** (**10–12**) in toluene. Inset: fluorescence images of the solutions under 365 nm UV illumination ($c = 5 \times 10^{-4}$ M, measured in air). The emission peaks of **7** are 457 nm and 596 nm; the emission peaks of **10** are 432 nm and 595 nm.

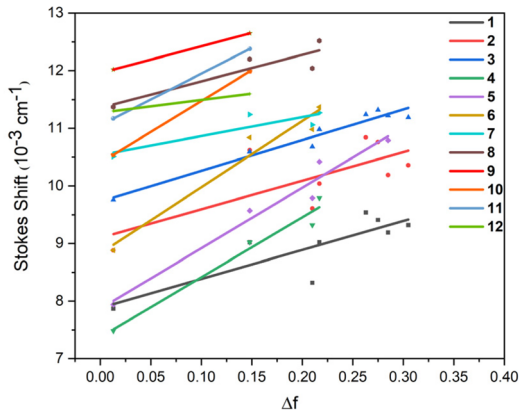

Fig. 3 Lippert–Mataga plot with linear fitting of cyanobenzene phenothiazine derivatives **1–12**.

delocalization. This constraint prevents an increase in the number of phenothiazine units from amplifying the dipole moment difference, thereby leading to the anomalous slope behavior of **12** within the **PTHIPN** series. Additionally, a greater number of phenothiazine and cyano groups correlates with a larger Stokes displacement, consistent with the enhanced solvent polarity response induced by stronger intramolecular charge transfer.

Despite comparable emission wavelengths across the series, all synthesized compounds exhibited low solution-phase quantum yields in air-saturated toluene (φ = 0.3–7.5%), indicating efficient nonradiative decay pathways. However, a consistent enhancement in φ was observed when they were measured under a nitrogen atmosphere (0.7–19.4%, Table S14). This collective improvement in photophysical properties under oxygen-free conditions indicates that the emission pathway is susceptible to oxygen quenching, likely involving triplet states. Fluorescence lifetime in toluene ranged from 2.11 to 19.35 ns (Fig. S108–S122).

Theoretical studies were performed using a toluene solution model of cyanobenzene–phenothiazine fluorescent molecules, with the PBE1PBE method employed for structural optimization and TD-DFT calculations under the IEFPCM solvation model. Ground-state optimization was completed at the 6-31G(d,p) basis set level, while excited-state TD-DFT calculations adopted the 6-311G(d,p) basis set. As shown in Fig. 4, the HOMO/LUMO orbital distribution reveals a clear intramolecular separation, with the HOMO localized on the phenothiazine donor and the LUMO on the cyanobenzene acceptor. This is in direct contrast to difluoroboranyl systems, in which the phenylene spacer acts as a secondary donor.[55] In PTHBNs and PTHIPNs, the extended benzene ring, coupled with the cyanobenzene, is predominantly involved in the LUMO, exhibiting an electron-withdrawing nature. This demonstrates that the electronic role of a π-spacer is not intrinsic but is critically determined by the chemical environment. Notably, in **3**, the para-substituted quasi-axial conformation of the phenothiazine unit contributes to the LUMO but not the HOMO, undercoring the essential role of molecular conformation in modulating the electronic properties.

A key computational finding is the consistent decrease in both the HOMO–LUMO energy gap and the $S_0 \rightarrow S_1$ vertical

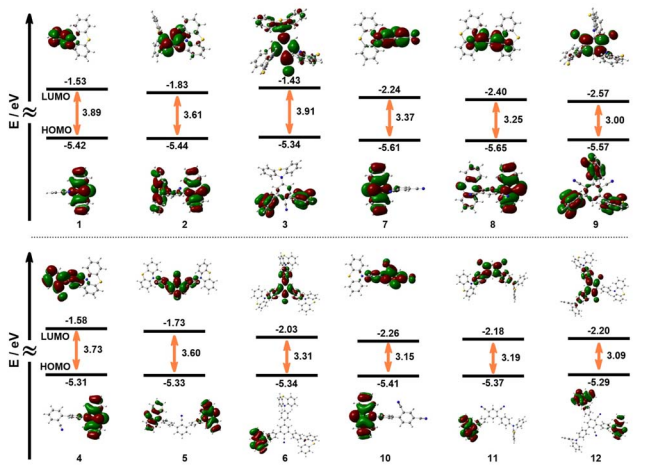

Fig. 4 The HOMO/LUMO of cyanobenzene phenothiazine derivatives **1-12**, calculated by the DFT method at the 6-31G(d,p) basis set level of theory.

excitation energy with an increasing number of donor–acceptor (D–A) pairs. This trend directly correlates with and explains the experimentally observed redshift in the fluorescence emission spectra. Furthermore, the energy gaps between the first singlet and triplet excited states (ΔE_{ST}) were found to be less than 0.3 eV for all compounds except for structure **12** (Table S16). This small ΔE_{ST} supports the idea that triplet states can undergo reverse intersystem crossing (RISC). Although the lifetime data in toluene solution are not consistent with TADF, the solid-state packing may potentially enable a thermally activated delayed fluorescence (TADF) mechanism.

Additional analyses validated our computational approach. The natural transition orbital (NTO) analysis of the excited state provided a clearer picture of the actual orbital contributions to the transition, distinguishing them from the simple HOMO–LUMO picture (Table S15). Moreover, the ultraviolet absorption spectrum simulated from the optimized ground-state structures successfully reproduced the experimental trend (Fig. S172). The above theoretical results verify that increasing the number of adjacent D–A pairs on the central benzene ring enhances the ICT effect, narrows the energy gap, and ultimately leads to a redshift in the emission spectrum.

Solid-state fluorescence characterization revealed pronounced structure-dependent emission tuning. Analysis of powdered samples revealed marked variations in photophysical properties, governed by the proportion and connectivity of the PTZ and cyano groups. Specifically, structural modifications induced bathochromic shifts across a broad emission range from 462 to 677 nm (Fig. 5, S128, S131 and S132). CIE coordinate analysis (Fig. S136) categorized the compounds into three distinct chromatic groups, namely derivatives **5**, **1**, and **4** emitted in the blue-green region (λ_{em} = 463–489 nm), while compounds **7**, **2**, **6**, **3**, **10**, and **11** displayed yellow fluorescence (λ_{em} = 515–579 nm). Notably, **12**, **8**, and **9** exhibited orange-to-red emission (λ_{em} = 597–677 nm), marking the longest wavelengths within the series. A notable bathochromic shift emerged as the number of cyano substituents increased while maintaining the PTZ donor counts, indicative of reduced S_1-state energy levels.

Varying PTZ donor units while maintaining cyanobenzene acceptors also induced progressive bathochromic shifts in emission wavelengths for all derivatives except **4** and **5** ($\Delta\lambda_{em}$ = 50–120 nm), with the number of PTZ groups serving as a critical regulator of emission wavelength. Solid-state quantum yields (Φ_F) spanned 0.9% (**1**), 2.9% (**2**), 4% (**3**), 1.8% (**4**), 5% (**5**), 18.6% (**6**), 39.7% (**7**), 2.0% (**8**), 2.0% (**9**), 18.1% (**10**), 15.8% (**11**) and 20.6% (**12**) respectively (Fig. S135). As evidenced by photophysical evaluations, structural extension *via* the phenylene π-conjugation bridge between phenothiazine donors and cyanobenzene acceptors resulted in a 2- to 10-fold enhancement of quantum yields compared to non-extended derivatives. However, the diminished fluorescence quantum yields of cyanobenzene phenothiazine derivatives in both solution and the solid phase may be attributed to intramolecular/intermolecular resonance energy transfer,[56–59] with enhanced efficiency in the condensed phase due to molecular packing.

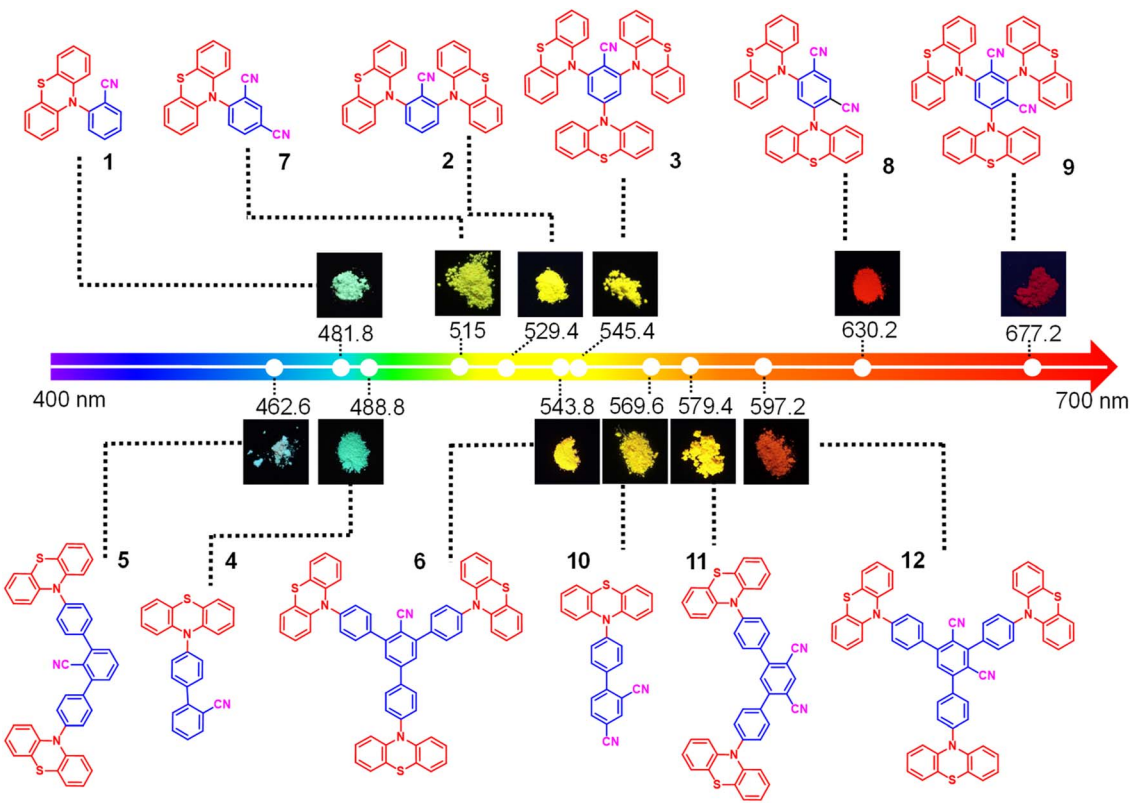

Fig. 5 Solid-state maximum emission wavelengths and fluorescence images of cyanobenzene phenothiazine derivatives **1–12**.

Table 1 Photophysical data of **1–12** in the solid state[a]

Compound	λ_{em} (nm)	φ_F (%)	τ (ns)	K_r (s^{-1})	K_{nr} (s^{-1})
o-PTZBN (**1**)	482	0.9	11.00	8.1×10^5	9.0×10^7
2,6-2PTZBN (**2**)	529	2.9	501.50	5.78×10^4	1.94×10^6
2,4,6-3PTZBN (**3**)	545	4.0	761.47	5.25×10^4	1.26×10^6
o-PTHBN (**4**)	489	1.8	2.70	6.67×10^6	3.64×10^8
2,6-2PTHBN (**5**)	463	5.0	3.39	1.48×10^7	2.80×10^8
2,4,6-3PTHBN (**6**)	544	18.6	466.73	3.98×10^5	1.74×10^6
4-PTZIPN (**7**)	515	39.7	1261.32	3.15×10^5	4.8×10^5
4,6-2PTZIPN (**8**)	630	2.0	99.41	2.0×10^5	9.86×10^6
2,4,6-3PTZIPN (**9**)	677	2.0	3.52	5.68×10^5	2.78×10^8
4-PTHIPN (**10**)	570	18.1	265.92	6.8×10^5	3.08×10^6
4,6-2PTHIPN (**11**)	579	15.8	589.20	2.68×10^5	1.43×10^6
2,4,6-3PTHIPN (**12**)	597	20.6	725.71	2.84×10^5	1.09×10^6

[a] The λ_{ex} of cyanobenzene phenothiazine derivatives **1–12** is 370 nm. Radiative decay rate constant $k_r = \varphi/\tau$. Nonradiative decay rate constant $k_{nr} = (1 - \varphi)/\tau$.

Fluorescence lifetime measurements of solid-state samples revealed a broad distribution spanning 2.70 ns to 1261.32 ns. As shown in Table 1, the incorporation of PTZ or PTH units into the cyanobenzene system significantly enhanced the fluorescence lifetimes: the lifetime of **1** increased from 11.00 ns to 761.47 ns for **3**, and that of **4** increased from 2.70 ns to 466.73 ns for **6**. In the 1,3-dicyanobenzene system, the introduction of PTH units also improved lifetimes—**10** increased from 265.92 ns to 725.71 ns. However, the incorporation of PTZ units in this system drastically reduced the lifetimes, dropping sharply from 1261.32 ns (**7**) to 3.52 ns (**9**). Notably, compounds **2**, **3**, **6**, **7**, **10**, **11**, and **12** displayed distinct dual-exponential decays, suggesting TADF properties (Fig. S138–S151). On the other hand, the lifetime of **2** significantly increased from 501 ns in the powder state to 5240.72 ns in the crystalline state, demonstrating the crucial influence of intermolecular interactions and molecular packing on fluorescence lifetimes. For the other compounds, the variation trend of crystalline-state lifetimes with molecular structure was consistent with that in the powder state (Fig. S152–S165).

Characterization of crystal structures provides critical insights into molecular conformations, noncovalent interactions, and packing motifs—key factors that together regulate the photophysical properties of organic luminescent materials. For such systems, quantum yield is determined not only by intrinsic molecular structure but also by conformational features and intermolecular arrangements in condensed phases (crystal/powder). Specifically, the rigid framework and dense packing in defect-free crystals impose spatial constraints that limit molecular vibrational/rotational motions, stabilizing thermodynamically favored conformations and suppressing nonradiative relaxation pathways—this partially modulates fluorescence lifetimes and φ_F.[60–62] In this study, X-ray diffraction (XRD) confirmed the structural integrity of all derivatives (Fig. S95–S106), and crystals exhibited distinct φ_F values compared to their powdered counterparts (Fig. S136).

Canonical J-aggregation is characterized by a head-to-tail dipole alignment of chromophores, which typically results in red-shifted emission, a narrower spectral bandwidth, and enhanced molar absorption coefficients. In contrast, non-canonical J-aggregation motifs deviate from this strict dipole orientation while retaining the aggregation-induced emission enhancement feature associated with J-aggregates. For the cyanobenzene phenothiazine system, **7** maintains high photoluminescent performance in both powdered ($\varphi_F = 39.7\%$, $\tau =$ 1261.32 ns) and crystalline states ($\varphi_F = 16.5\%$, $\tau = 1151.94$ ns), achieving its maximum quantum yield through J-aggregation sustained by four cooperative intermolecular interactions *via* C–H···S contacts (2.976 Å), cyano C≡N···H–C dipole alignments (2.602–2.705 Å), and edge-to-face π–π stacking (2.875 Å), as structurally resolved in Fig. 6.[63,64]

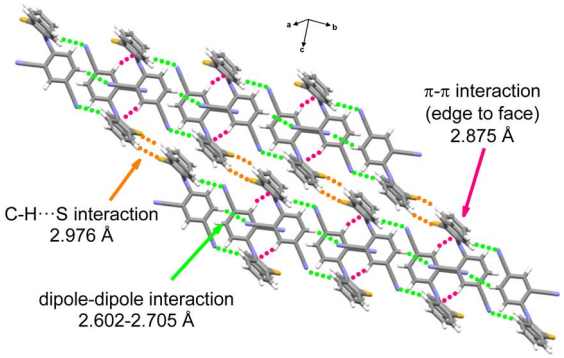

Fig. 6 Intermolecular weak interactions in the crystal **7**.

Notably, **3** exhibited a large fluorescence lifetime of 1.10 μs, and a doubled quantum yield, with φ_F increasing from 4.0% in powder to 8.0% in crystal. This phenomenon is attributed to a three-pronged intermolecular interactions assembly comprising PTZ-directed π–π stacking with offset face-to-face distances of 3.381–3.451 Å and edge-to-face distances of 2.879–2.897 Å, cyano C≡N···H–C dipole alignment at 2.531 Å, and C–H···S orbital overlap ranging from 2.999 to 3.323 Å (Fig. 7c). The weak intermolecular forces drive a non-canonical J-aggregation motif with a densely packed pattern (Fig. 7b), which rigidifies molecular conformations to suppress nonradiative decay while promoting radiative recombination,[65] thereby extending fluorescence lifetimes and elevating quantum yields.

Beyond packing effects, conformational features in molecules also play a critical role in regulating luminescence properties. Specifically, the PTZ unit not only influences but also indicates molecular packing and exhibits stereochemical features, contributing to the facial chirality observed in the system. As shown in Fig. 7a, single-crystal analysis of **3** revealed the coexistence of enantiomers within the unit cell, confirming the existence of chirality. In the unit cell, PTZ moieties display distinct conformational preferences, namely that the *para*-cyano PTZ adopts a quasi-axial conformation, which is oriented perpendicular to the cyanobenzene plane, while the *ortho*-cyano PTZ units adopt quasi-equatorial conformations arranged spirally along the same direction. These stereochemical spatial arrangements result in non-superimposable mirror-image

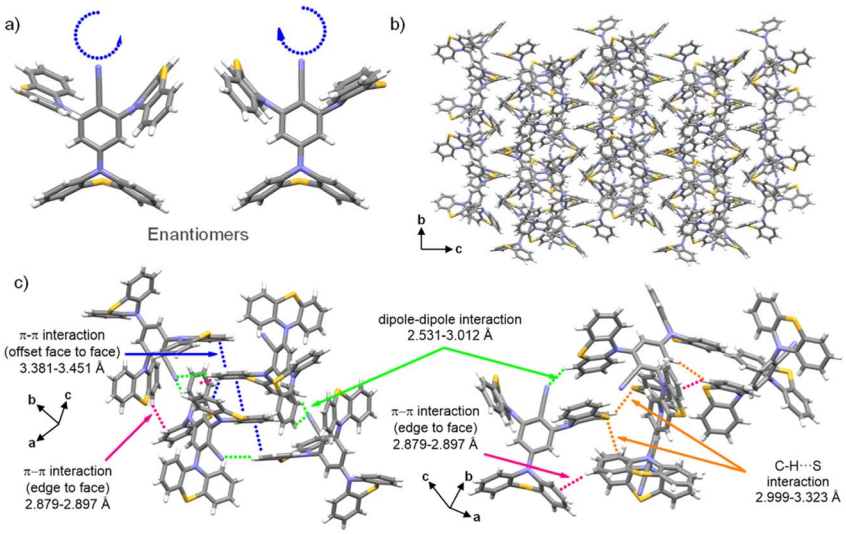

Fig. 7 (a) Enantiomers of structure **3**; (b) arrangement pattern of crystal **3** along the (100) direction; (c) intermolecular weak interactions in the crystal **3**.

pairs, with intrinsic facial chirality from conformation-driven spatial non-overlap.

Derivative **9** (Fig. 8a) was strategically designed by introducing an additional cyano group on **3**. This modification results in a propeller-like molecular architecture, in which all three PTZ units adopt quasi-equatorial conformations, with the sulfur atoms bent uniformly, forming a helical supramolecular assembly (Fig. 8b). As shown in Fig. 8c, the intermolecular edge-to-face π–π stacking (2.848–2.898 Å) between adjacent PTZ moieties and dipole–dipole interactions (2.397–2.832 Å) involving dichloromethane solvent molecules drive columnar cross-stacking. Each column exhibits a six-molecule helical repeat unit forming the $P6_1$ space group, where successive molecules rotate 60° along the column axis, completing a 360° cycle after six units. Notably, nitrogen atoms of cyano groups trace intertwined double-helical pathways (Fig. 8b). As shown in Fig. S82, inter-columnar edge-to-face π–π interactions (2.786–2.862 Å) and solvent-mediated dipole alignments (2.397–2.626 Å) further stabilize this columnar helical staggered packing, enhancing transition dipole coupling to promote irradiative decay.[66]

In terms of fluorescence lifetime, the crystalline state of **9** exhibits a shorter lifetime (3.52 ns) compared to its powder state (11.48 ns). This trend of reduced lifetime in the crystalline

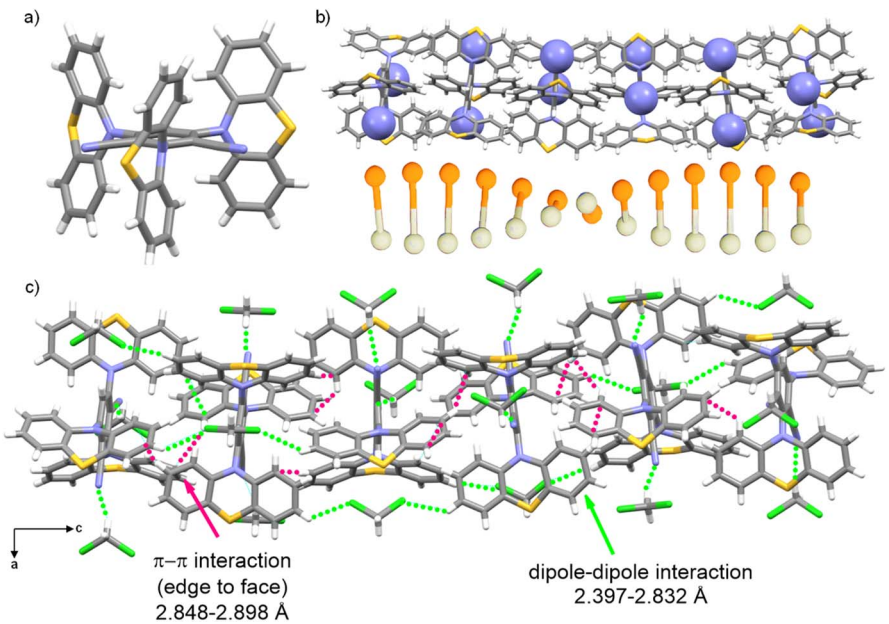

Fig. 8 (a) Crystal structure of **9**; (b) arrangement pattern of crystal **9** along the (010) direction (space-filling representation of the cyano nitrogen atom); (c) diagram of intermolecular weak interactions in the crystal **9**.

Table 2 Photophysical data of comparisons

Compound	λ_{em}	φ^a (%)	τ_p (ns)	τ_d (μs)	k_r (10^7 s^{-1})
4CzIPN[b]	507	21/86	17.8	5.1	1.8
m-3CzIPN[b]	426	12/86	7.9	26.1	1.5
4-PTZBN[c]	513	—	4610	44.2	—
Diarylboryl-PTZ[d]	485	20	5.11	5.07	3.9

[a] Photoluminescence quantum efficiency of the solution sample before/after Ar bubbling. [b] Measured in toluene. [c] Measured in film, $\tau_{phosphorescence} = 487.7$ μs. [d] Solid-state luminescence properties.

phase may be closely related to its unique molecular conformation. Specifically, the adoption of quasi-equatorial conformations by all PTZ units introduces significant steric hindrance to molecular rotation and vibration. Such constrained motion likely narrows the energy gaps between adjacent electronic states, facilitating nonradiative decay pathways through enhanced state mixing. Additionally, the compact columnar helical staggered packing strengthens intermolecular interactions, which may further promote nonradiative energy dissipation *via* intramolecular vibration–lattice vibration coupling and direct intermolecular energy transfer.[67] In contrast, the powder state features looser, more disordered packing with weaker intermolecular interactions and reduced steric constraints on PTZ units, leading to less efficient nonradiative decay and thus a longer lifetime.

To place our findings in the context of existing research, we compared the basic photophysical properties of our non-doped cyanobenzene–phenothiazine dyes with several established high-performance emitters, as summarized in Table 2. While impressive efficiencies have been reported for doped phenothiazine systems[68,69] and those incorporating *ortho*-substituents for conformational control,[51] the performance of non-doped phenothiazine donors is highly dependent on the overall molecular structure and the strength of the electron acceptor. For example, when comparing our compounds with the benchmark carbazole-isophthalonitrile series (*e.g.*, **4CzIPN** and ***m*-3CzIPN**)[40,70] and other phenothiazine-based analogues (*e.g.*, **4-PTZBN** and **Diarylboryl-PTZ**),[71,72] our derivatives exhibit competitive bathochromic-shift maximum emission wavelength, quantum yield, and emission lifetime. These comparisons underscore that our molecular engineering strategy—focusing on the systematic increase of adjacent D–A pairs and precise conformation-aggregation dual control—effectively enhances the luminescence efficiency and stability.

Conclusions

In summary, we discovered that by systematically regulating the number and relative positions of cyano groups and phenothiazine substituents on the central benzene ring, conformation-dependent electronic interactions and aggregation-induced packing effects cooperatively modulate the fluorescence properties of cyanobenzene phenothiazine derivatives. This establishes a conformation-aggregation dual regulation strategy for organic optoelectronics, where substituent engineering provides a fundamental basis for manipulating key photophysical regulatory pathways. In derivative **7**, multiple intermolecular interactions in J-aggregation synergistically promote the solid-state fluorescence quantum yield to the maximum value. In structure **3**, the quasi-axial conformation of the phenothiazine chromophore participates in the LUMO distribution. Coupled with intermolecular weak interactions, this leads to an order-of-magnitude enhancement in the crystalline-state fluorescence lifetime. In compound **9**, the introduction of *meta*-dicyano substitution modulates the conformational arrangement of three intramolecular phenothiazine units and their excited-state electronic distribution. This promotes columnar helical packing *via* intermolecular interactions, thereby tuning the competition between radiative and non-radiative decay pathways, ultimately achieving NIR solid-state fluorescence at 677 nm. Future studies will focus on both the application of cyanobenzene phenothiazine derivatives as organic photocatalysts and the conformational engineering of luminescent materials by extending this strategy to diverse donor–acceptor systems, especially three-dimensionally aromatic *o*-carborane-based systems, and investigating their stimuli-responsive dynamic conformational switching, such as temperature, pressure, and mechanical force, to develop high-performance emissive materials.

Conflicts of interest

There are no conflicts to declare.

Data availability

CCDC 2473370 for PTH-Bpin (starting material), 2474330 for *o*-PTZBN (**1**), 2474283 for 2,6-2PTZBN (**2**), 2474284 for 2,4,6-3PTZIPN (**3**), 2474288 for 4-PTZIPN (**7**), 2474289 for 4,6-2PTZIPN (**8**), 2474290 for 2,4,6-3PTZIPN (**9**), 2474286 for *o*-PTHBN (**4**), 2474287 for 2,6-2PTHBN (**5**), 2474291 for 4-PTHIPN (**10**), 2474293 for 4,6-2PTHIPN (**11**) contain the supplementary crystallographic data for this paper.[73]

The data supporting this article have been included as part of the supplementary information (SI). Supplementary information is available. See DOI: https://doi.org/10.1039/d5sc06095h.

Acknowledgements

This work was supported by the National Natural Science Foundation of China (No. U23A2078, 22171246, 22473100, and 22201268) and the Open Research: Fund of the State Key Laboratory of Coordination Chemistry, School of Chemistry and Chemical Engineering, Nanjing University. We would like to acknowledge Prof. Li-Jie Liu from Henan Agricultural University for his support in the quantum yield and lifetime measurements of this work and the valuable discussion.

Notes and references

1 S. Y. Lee, T. Yasuda, Y. S. Yang, Q. Zhang and C. Adachi, Luminous Butterflies: Efficient Exciton Harvesting by

Benzophenone Derivatives for Full-Color Delayed Fluorescence OLEDs, *Angew. Chem., Int. Ed.*, 2014, **53**, 6402–6406.

2 C. Maeda, T. Todaka, T. Ueda and T. Ema, Color-Tunable Solid-State Fluorescence Emission from Carbazole-Based BODIPYs, *Chem.–Eur. J.*, 2016, **22**, 7508–7513.

3 Z. Xiang, Z.-Y. Wang, T.-B. Ren, W. Xu, Y.-P. Liu, X.-X. Zhang, P. Wu, L. Yuan and X.-B. Zhang, A general strategy for development of a single benzene fluorophore with full-color-tunable, environmentally insensitive, and two-photon solid-state emission, *Chem. Commun.*, 2019, **55**, 11462–11465.

4 R. Furue, T. Nishimoto, I. S. Park, J. Lee and T. Yasuda, Aggregation-Induced Delayed Fluorescence Based on Donor/Acceptor-Tethered Janus Carborane Triads: Unique Photophysical Properties of Nondoped OLEDs, *Angew. Chem., Int. Ed.*, 2016, **55**, 7171–7175.

5 J. Lu, B. Pattengale, Q. Liu, S. Yang, W. Shi, S. Li, J. Huang and J. Zhang, Donor–Acceptor Fluorophores for Energy-Transfer-Mediated Photocatalysis, *J. Am. Chem. Soc.*, 2018, **140**, 13719–13725.

6 K.-L. Woon, P. A. Nikishau and G. Sini, Fast and Accurate Determination of the Singlet–Triplet Gap in Donor–Acceptor and Multiresonance TADF Molecules by Using Hole–Hole Tamm–Dancoff Approximated Density Functional Theory, *Adv. Theory Simul.*, 2022, **5**, 2200056.

7 L. Chen, C. Li, E. Fu, M. Li, Y. Kuboi, Z.-Y. Li, Z. Chen, J. Chen, X. Liu, X. Tang, L. Frédéric, F. Maurel, C. Adachi, F. Mathevet and S. Zhang, A Donor–Acceptor Cage for Thermally Activated Delayed Fluorescence: toward a New Kind of TADF Exciplex Emitters, *ACS Mater. Lett.*, 2023, **5**, 1450–1455.

8 Y. Tao, K. Yuan, T. Chen, P. Xu, H. Li, R. Chen, C. Zheng, L. Zhang and W. Huang, Thermally Activated Delayed Fluorescence Materials Towards the Breakthrough of Organoelectronics, *Adv. Mater.*, 2014, **26**, 7931–7958.

9 H. M. Kim and B. R. Cho, Small-Molecule Two-Photon Probes for Bioimaging Applications, *Chem. Rev.*, 2015, **115**, 5014–5055.

10 Z. Yang, Z. Mao, Z. Xie, Y. Zhang, S. Liu, J. Zhao, J. Xu, Z. Chi and M. P. Aldred, Recent advances in organic thermally activated delayed fluorescence materials, *Chem. Soc. Rev.*, 2017, **46**, 915–1016.

11 J. Yoo, I. T. Kim, J. Y. Park and Y.-R. Kim, Electrochemical glucose sensor based on a phenothiazine derivative mediator with nicotinamide adenine dinucleotide-dependent glucose dehydrogenase, *Sens. Actuators, B*, 2025, **422**, 136630–136640.

12 J.-M. Wang, T.-C. Lee, C.-C. Chung, W.-Y. Chen, S.-Y. Wu, Y.-D. Lin, Y. J. Chang, C.-W. Lu and C.-H. Chang, Toward ultra-high efficiency tandem OLEDs: Benzothiazole-based bipolar hosts and specific device architectures, *Chem. Eng. J.*, 2023, **472**, 145023–145035.

13 X. Su, Y. Liu, Y. Zhong, P. Shangguan, J. Liu, Z. Luo, C. Qi, J. Guo, X. Li, D. Lin, G. Wang, D. Wang, T. Han, J. Wang, B. Shi and B. Z. Tang, A Brain-Targeting NIR-II Polymeric Phototheranostic Nanoplatform toward Orthotopic Drug-Resistant Glioblastoma, *Nano Lett.*, 2025, **25**, 3445–3454.

14 Z. Xu, M. Lv, J. Yang, T. Li, J. Lv, J. Li, H. Xiao, Y. Yang, S. Zhou, X. Tan, L. Cheng, H. Guo, L. Xi, P.-L. Shao and B. Zhang, An Efficient Heat and Peroxynitrite Generating Nanoplatform for Multimodal Imaging-guided Precision Tumor Phototherapy, *Aggregate*, 2025, **6**, e70040.

15 H. Wang, C. Peng, M. Chen, Y. Xiao, T. Zhang, X. Liu, Q. Chen, T. Yu and W. Huang, Wide-Range Color-Tunable Organic Scintillators for X-Ray Imaging Through Host-Guest Doping, *Angew. Chem., Int. Ed.*, 2024, **63**, e202316190.

16 M. Dong, A. Lv, X. Zou, N. Gan, C. Peng, M. Ding, X. Wang, Z. Zhou, H. Chen, H. Ma, L. Gu, Z. An and W. Huang, Polymorphism-Dependent Organic Room Temperature Phosphorescent Scintillation for X-Ray Imaging, *Adv. Mater.*, 2024, **36**, 2310663.

17 P. Huang, Manju, S. Kazim, L. Lezama, R. Misra and S. Ahmad, Tailoring of a Phenothiazine Core for Electrical Conductivity and Thermal Stability: Hole-Selective Layers in Perovskite Solar Cells, *ACS Appl. Mater. Interfaces*, 2021, **13**, 33311–33320.

18 C. Zhang, Z. Niu, S. Peng, Y. Ding, L. Zhang, X. Guo, Y. Zhao and G. Yu, Phenothiazine-Based Organic Catholyte for High-Capacity and Long-Life Aqueous Redox Flow Batteries, *Adv. Mater.*, 2019, **31**, 1901052–1901060.

19 H. Bildirir, D. Alván, N. Patil, V. A. de la Peña O'Shea, M. Liras and R. Marcilla, Hypercrosslinked Phenothiazine Polymer as a Low-Cost and Durable Organic Cathode for Rechargeable Lithium Batteries, *ACS Appl. Polym. Mater.*, 2024, **6**, 10092–10101.

20 M. Zhang, T. Li, X. Liu, C. Zhang and X. Li, Molecular Revealing the High-stable Polycyclic Azine Derivatives for Long-Lifetime Aqueous Organic Flow Batteries, *Adv. Funct. Mater.*, 2023, **34**, 2312608–2312616.

21 R. K. Gautam, X. Wang, S. Sinha and J. J. Jiang, Triphasic Electrolytes for Membrane-Free High-Voltage Redox Flow Battery, *ACS Energy Lett.*, 2024, **9**, 218–225.

22 X. Pan, C. Fang, M. Fantin, N. Malhotra, W. Y. So, L. A. Peteanu, A. A. Isse, A. Gennaro, P. Liu and K. Matyjaszewski, Mechanism of Photoinduced Metal-Free Atom Transfer Radical Polymerization: Experimental and Computational Studies, *J. Am. Chem. Soc.*, 2016, **138**, 2411–2425.

23 H. Wang and N. T. Jui, Catalytic Defluoroalkylation of Trifluoromethylaromatics with Unactivated Alkenes, *J. Am. Chem. Soc.*, 2018, **140**, 163–166.

24 F.-D. Lu, D. Liu, L. Zhu, L.-Q. Lu, Q. Yang, Q.-Q. Zhou, Y. Wei, Y. Lan and W.-J. Xiao, Asymmetric Propargylic Radical Cyanation Enabled by Dual Organophotoredox and Copper Catalysis, *J. Am. Chem. Soc.*, 2019, **141**, 6167–6172.

25 A. M. Martínez-Gualda, R. Cano, L. Marzo, R. Pérez-Ruiz, J. Luis-Barrera, R. Mas-Ballesté, A. Fraile, V. A. de la Peña O'Shea and J. Alemán, Chromoselective access to Z- or E-allylated amines and heterocycles by a photocatalytic allylation reaction, *Nat. Commun.*, 2019, **10**, 2634.

26 M. H. Aukland, M. Šiaučiulis, A. West, G. J. P. Perry and D. J. Procter, Metal-free photoredox-catalysed formal C–H/

C–H coupling of arenes enabled by interrupted Pummerer activation, *Nat. Catal.*, 2020, **3**, 163–169.

27 S. Shibutani, T. Kodo, M. Takeda, K. Nagao, N. Tokunaga, Y. Sasaki and H. Ohmiya, Organophotoredox-Catalyzed Decarboxylative C(sp3)–O Bond Formation, *J. Am. Chem. Soc.*, 2020, **142**, 1211–1216.

28 Y. Zhang, D. Jiang, Z. Fang, N. Zhu, N. Sun, W. He, C. Liu, L. Zhao and K. Guo, Photomediated core modification of organic photoredox catalysts in radical addition: mechanism and applications, *Chem. Sci.*, 2021, **12**, 9432–9441.

29 Y. Cai and T. Ritter, Meerwein-type Bromoarylation with Arylthianthrenium Salts, *Angew. Chem., Int. Ed.*, 2022, **61**, e202209882.

30 M. Nakagawa, Y. Matsuki, K. Nagao and H. Ohmiya, A Triple Photoredox/Cobalt/Brønsted Acid Catalysis Enabling Markovnikov Hydroalkoxylation of Unactivated Alkenes, *J. Am. Chem. Soc.*, 2022, **144**, 7953–7959.

31 S. Halder, S. Mandal, A. Kundu, B. Mandal and D. Adhikari, Super-Reducing Behavior of Benzo[b]phenothiazine Anion Under Visible-Light Photoredox Condition, *J. Am. Chem. Soc.*, 2023, **145**, 22403–22412.

32 O. P. Williams, A. F. Chmiel, M. Mikhael, D. M. Bates, C. S. Yeung and Z. K. Wickens, Practical and General Alcohol Deoxygenation Protocol, *Angew. Chem., Int. Ed.*, 2023, **62**, e202300178.

33 P. Seefeldt, A. Villinger and M. Brasholz, Photoredox-Catalyzed Carbon Radical Generation from α-Keto-N,O-acetals: Synthesis of Functionalized Azepino[1,2-a]indoles and Azepino[1,2-a]furo[3,2-b]indoles, *Adv. Synth. Catal.*, 2024, **366**, 24–30.

34 N. Hölter, N. H. Rendel, L. Spierling, A. Kwiatkowski, R. Kleinmans, C. G. Daniliuc, O. S. Wenger and F. Glorius, Phenothiazine Sulfoxides as Active Photocatalysts for the Synthesis of γ-Lactones, *J. Am. Chem. Soc.*, 2025, **147**, 12908–12916.

35 S. Xu, H. Zhang, J. Zong, H. Cao, D. Tu, C.-s. Lu and H. Yan, Taming Inert B–H Bond with Low Energy Light: A Near-Infrared Light-Induced Approach to Facile Carborane Cluster-Amino Acid Coupling, *J. Am. Chem. Soc.*, 2025, **147**, 12845–12857.

36 J. Zhao, H. Yu, X. Jin, B. Qin, S. Mei, J.-F. Xu and X. Zhang, Radical-mediated click-clip reactions, *Science*, 2024, **385**, 1354–1359.

37 J. Han, C. A. Haines, J. J. Piane, L. L. Filien and E. D. Nacsa, An Electrochemical Design for Catalytic Dehydration: Direct, Room-Temperature Esterification without Acid or Base Additives, *J. Am. Chem. Soc.*, 2023, **145**, 15680–15687.

38 N. Akai, S. Kudoh and M. Nakata, Lowest excited triplet states of 1,2- and 1,4-dicyanobenzenes by low-temperature matrix-isolation infrared spectroscopy and density-functional-theory calculation, *Chem. Phys. Lett.*, 2003, **371**, 655–661.

39 K. R. Justin Thomas, M. Velusamy, J. T. Lin, Y. T. Tao and C. H. Chuen, Cyanocarbazole Derivatives for High-Performance Electroluminescent Devices, *Adv. Funct. Mater.*, 2004, **14**, 387–392.

40 H. Uoyama, K. Goushi, K. Shizu, H. Nomura and C. Adachi, Highly efficient organic light-emitting diodes from delayed fluorescence, *Nature*, 2012, **492**, 234–238.

41 X. Cao, D. Zhang, S. Zhang, Y. Tao and W. Huang, CN-Containing donor–acceptor-type small-molecule materials for thermally activated delayed fluorescence OLEDs, *J. Mater. Chem. C*, 2017, **5**, 7699–7714.

42 Y. Li, E. Huang, X. Guo and K. Feng, Cyano-functionalized organic and polymeric semiconductors for high-performance n-type organic electronic devices, *Mater. Chem. Front.*, 2023, **7**, 3803–3819.

43 G. M. Upadhyay, H. M. Mande, D. K. Pithadia, R. H. Maradiya and A. V. Bedekar, Effect of the Position of the Cyano Group on Molecular Recognition, Supramolecular Superhelix Architecture, and Spontaneous Resolution of Aza[7]helicenes, *Cryst. Growth Des.*, 2019, **19**, 5354–5361.

44 E. Juaristi and R. Notario, Density Functional Theory Computational Reexamination of the Anomeric Effect in 2-Methoxy- and 2-Cyano-1,3-dioxanes and 1,3-Dithianes. Stereoelectronic Interactions Involving the Cyano (C≡N:) Group Revealed by Natural Bond Orbital (NBO) Analysis, *J. Org. Chem.*, 2018, **83**, 10326–10333.

45 S. Scheiner, Versatility of the Cyano Group in Intermolecular Interactions, *Molecules*, 2020, **25**, 4495–4514.

46 S. K. Rai, T. Sierański, S. Khanam, K. R. Kumar, B. Sridhar and A. K. Tewari, Quantitative Analysis of Intermolecular Interactions in 3-Cyano-2-Pyridones: Evaluation through Single Crystal X-ray Diffraction and Density Functional Theory, *ChemistrySelect*, 2018, **3**, 5864–5873.

47 J. Yang, Z. Ren, B. Chen, M. Fang, Z. Zhao, B. Z. Tang, Q. Peng and Z. Li, Three polymorphs of one luminogen: how the molecular packing affects the RTP and AIE properties?, *J. Mater. Chem. C*, 2017, **5**, 9242–9246.

48 L. Mayer, L. May and T. J. J. Müller, The interplay of conformations and electronic properties in N-aryl phenothiazines, *Org. Chem. Front.*, 2020, **7**, 1206–1217.

49 F. Baraket, B. Pedras, É. Torres, M. J. Brites, M. Dammak and M. N. Berberan-Santos, Novel phenoxazine-benzonitrile and phenothiazine-benzonitrile donor-acceptor molecules with thermally activated delayed fluorescence (TADF), *Dyes Pigm.*, 2020, **175**, 108114.

50 Z. Wang, Y. Li, Y. Yang, Y. Chen and H. Wu, Intense mechanoluminescence in an organic donor-acceptor crystal: Grinding induced crystal-to-crystal phase transformation, *Opt. Mater.*, 2022, **123**, 111886.

51 M. Gao, R. Wu, Y. Zhang, Y. Meng, M. Fang, J. Yang and Z. Li, New Molecular Photoswitch Based on the Conformational Transition of Phenothiazine Derivatives and Corresponding Triplet Emission Properties, *J. Am. Chem. Soc.*, 2025, **147**, 2653–2663.

52 T. Liu, Y.-G. Wei, Y.-Q. Yuan and Q.-X. Guo, Charge Transfer in Excited Donor-acceptor Phenothiazine Derivatives, *Chin. J. Chem.*, 2005, **23**, 1430–1436.

53 Y. Wang, J. Feng, E.-Q. Li, Z. Jia and T.-P. Loh, Recent advances in ligand-enabled palladium-catalyzed divergent synthesis, *Org. Biomol. Chem.*, 2024, **22**, 37–54.

54 L. Rasu, M. Amiri and S. H. Bergens, Carbazole–Cyanobenzene Dyes Electrografted to Carbon or Indium-Doped Tin Oxide Supports for Visible Light-Driven Photoanodes and Olefin Isomerizations, *ACS Appl. Mater. Interfaces*, 2021, **13**, 17745–17752.

55 A. M. Grabarz, A. D. Laurent, B. Jędrzejewska, A. Zakrzewska, D. Jacquemin and B. Ośmiałowski, The Influence of the π-Conjugated Spacer on Photophysical Properties of Difluoroboranyls Derived from Amides Carrying a Donor Group, *J. Org. Chem.*, 2016, **81**, 2280–2292.

56 D. J. Hurley and Y. Tor, Donor/Acceptor Interactions in Systematically Modified RuII−OsII Oligonucleotides, *J. Am. Chem. Soc.*, 2002, **124**, 13231–13241.

57 S. Faure, C. Stern, R. Guilard and P. D. Harvey, Role of the Spacer in the Singlet−Singlet Energy Transfer Mechanism (Förster vs. Dexter) in Cofacial Bisporphyrins, *J. Am. Chem. Soc.*, 2004, **126**, 1253–1261.

58 J. Lee, U. Jo and J. Y. Lee, Suppression of Dexter Energy Transfer through Modulating Donor Segments of Thermally Activated Delayed Fluorescence Assistant Dopants, *ACS Appl. Mater. Interfaces*, 2023, **15**, 21261–21269.

59 U. Deori, G. P. Nanda, C. Murawski and P. Rajamalli, A perspective on next-generation hyperfluorescent organic light-emitting diodes, *Chem. Sci.*, 2024, **15**, 17739–17759.

60 J. Yang, X. Zhen, B. Wang, X. Gao, Z. Ren, J. Wang, Y. Xie, J. Li, Q. Peng, K. Pu and Z. Li, The influence of the molecular packing on the room temperature phosphorescence of purely organic luminogens, *Nat. Commun.*, 2018, **9**, 840–850.

61 S. Tian, H. Ma, X. Wang, A. Lv, H. Shi, Y. Geng, J. Li, F. Liang, Z.-M. Su, Z. An and W. Huang, Utilizing d–pπ Bonds for Ultralong Organic Phosphorescence, *Angew. Chem., Int. Ed.*, 2019, **58**, 6645–6649.

62 J. Ren, Y. Wang, Y. Tian, Z. Liu, X. Xiao, J. Yang, M. Fang and Z. Li, Force-Induced Turn-On Persistent Room-Temperature Phosphorescence in Purely Organic Luminogen, *Angew. Chem., Int. Ed.*, 2021, **60**, 12335–12340.

63 W. Li, W. Li, L. Gan, M. Li, N. Zheng, C. Ning, D. Chen, Y.-C. Wu and S.-J. Su, J-Aggregation Enhances the Electroluminescence Performance of a Sky-Blue Thermally Activated Delayed-Fluorescence Emitter in Nondoped Organic Light-Emitting Diodes, *ACS Appl. Mater. Interfaces*, 2020, **12**, 2717–2723.

64 N. Liu, S. He, Z. Cheng and J. Hu, Enhancing the fluorescence emission of the NIR-II fluorophores: Strategies, mechanisms, challenges, and opportunities, *Coord. Chem. Rev.*, 2025, **532**, 216511.

65 O. P. Dimitriev, Dynamics of Excitons in Conjugated Molecules and Organic Semiconductor Systems, *Chem. Rev.*, 2022, **122**, 8487–8593.

66 U. Petralanda, G. Biffi, S. C. Boehme, D. Baranov, R. Krahne, L. Manna and I. Infante, Fast Intrinsic Emission Quenching in Cs4PbBr6 Nanocrystals, *Nano Lett.*, 2021, **21**, 8619–8626.

67 Q. Wen, N. Malik, Y. Addadi, M. Weißenfels, V. Singh, L. J. W. Shimon, M. Lahav and M. E. van der Boom, Energy Transport in Dichroic Metallo-organic Crystals: Selective Inclusion of Spatially Resolved Arrays of Donor and Acceptor Dyes in Different Nanochannels, *Angew. Chem., Int. Ed.*, 2023, **62**, e202214041.

68 Y. Tian, J. Yang, Z. Liu, M. Gao, X. Li, W. Che, M. Fang and Z. Li, Multistage Stimulus-Responsive Room Temperature Phosphorescence Based on Host–Guest Doping Systems, *Angew. Chem., Int. Ed.*, 2021, **60**, 20259–20263.

69 Y. Wang, J. Yang, M. Fang, Y. Gong, J. Ren, L. Tu, B. Z. Tang and Z. Li, New Phenothiazine Derivatives That Exhibit Photoinduced Room-Temperature Phosphorescence, *Adv. Funct. Mater.*, 2021, **31**, 2101719.

70 H. ANoda, X.-K. Chen, H. Nakanotani, T. Hosokai, M. Miyajima, N. Notsuka, Y. Kashima, J.-L. Brédas and C. Adachi, Critical role of intermediate electronic states for spin-flip processes in charge-transfer-type organic molecules with multiple donors and acceptors, *Nat. Mater.*, 2019, **18**, 1084–1090.

71 X. Guo, J. Yang, P. Yuan, Y. Wang, X. Qiao, Z. Li, B. Z. Tang and D. Ma, High Efficiency Non-Doped Organic Light Emitting Diodes Based on Pure Organic Room Temperature Phosphorescence by High-Lying Singlet Exciton Fission, *Laser Photonics Rev.*, 2024, **19**, 2401015–2401023.

72 K. K. Neena, P. Sudhakar, K. Dipak and P. Thilagar, Diarylboryl-phenothiazine based multifunctional molecular siblings, *Chem. Commun.*, 2017, **53**, 3641–3644.

73 CCDC 2473370: Experimental Crystal Structure Determination, 2025, DOI: 10.5517/ccdc.csd.cc2p0r4m; CCDC 2474330: Experimental Crystal Structure Determination, 2025, DOI: 10.5517/ccdc.csd.cc2p1r3m; CCDC 2474283: Experimental Crystal Structure Determination, 2025, DOI: 10.5517/ccdc.csd.cc2p1pl1; CCDC 2474284: Experimental Crystal Structure Determination, 2025, DOI: 10.5517/ccdc.csd.cc2p1pm2; CCDC 2474288: Experimental Crystal Structure Determination, 2025, DOI: 10.5517/ccdc.csd.cc2p1pr6; CCDC 2474289: Experimental Crystal Structure Determination, 2025, DOI: 10.5517/ccdc.csd.cc2p1ps7; CCDC 2474290: Experimental Crystal Structure Determination, 2025, DOI: 10.5517/ccdc.csd.cc2p1pt8; CCDC 2474286: Experimental Crystal Structure Determination, 2025, DOI: 10.5517/ccdc.csd.cc2p1pp4; CCDC 2474287: Experimental Crystal Structure Determination, 2025, DOI: 10.5517/ccdc.csd.cc2p1pq5; CCDC 2474291: Experimental Crystal Structure Determination, 2025, DOI: 10.5517/ccdc.csd.cc2p1pv9; CCDC 2474293: Experimental Crystal Structure Determination, 2025, DOI: 10.5517/ccdc.csd.cc2p1pxc.